Skid resistance of pavement surface aggregates in Quebec: effects of polishing time, wear mechanisms and aggregates properties.

Mbayang Kandji
PhD student
Université Laval
Québec, Québec
Mbayang.kandji.1@ulaval.ca

Benoit Fournier
Professor, research director
Université Laval
Québec, Québec
Benoit.fournier@ggl.ulaval.ca

Josée Duchesne
Professor, research director
Université Laval
Québec, Québec
Josee.Duchesne@ggl.ulaval.ca

Félix Doucet
Senior Pavement Materials Engineer
Ministère des Transports et de la Mobilité Durable du Québec (MTMD)
Québec, Québec
Felix.doucet@transports.gouv.qc.ca

Paper prepared for the session Designing, Building and Managing a Sustainable Pavement Network
2025 Transportation Association of Canada (TAC) Conference & Exhibition
Québec City, Québec

Acknowledgements

This research is supported by the Ministère des Transports et de la Mobilité Durable of Québec (MTMD). The authors are grateful to Stéphane Bouchard, Mélissa Roy Tremblay, Julie Francoeur, Solange Rodgers, Louise Faucher, Francis Plamondon, Michel Robert (MTMD) and Samy Essalik, Andrea Rodrigues, Pierre-Luc Fecteau, Nicholas Larouche, Armel Bakop Kamdem (Université Laval) for their contribution to the data collection.

Abstract

The MTMD LC 21-102 test method is an accelerated polishing by projection test, used in Quebec (Canada) to simulate the wear of coarse aggregates used in pavement surface layers, regarding skid resistance. Their suitability for use in construction is then evaluated by measuring their residual friction coefficient using a British pendulum. This study aims to investigate the effect of polishing time, better understand the wear mechanisms through microtexture evolution, identify the intrinsic properties of aggregates that govern polishing resistance and develop predictive models based on these influential properties. The research was carried out in two phases. The first focused on four aggregates and involved monitoring microtexture and friction parameters at incremental polishing stages. The second involved eighteen aggregates and focused on identifying the most influential properties using a broader dataset. The friction and microtexture parameters were measured before and after polishing. Mineralogical, petrographic and mechanical properties were assessed through optical microscopy, X-ray diffraction (XRD), Los Angeles and Micro-Deval tests. A 3D laser microprofilometer was used to capture the surface relief of aggregate particles and to determine their microtexture parameters such as peak density, shape and height. A British pendulum was used to measure the friction coefficient. The results show that the current standard polishing time may underestimate aggregate wear: friction continued to decrease beyond the specified duration, suggesting the need to extend the polishing time to reach maximum wear. Polishing by projection also revealed distinct wear mechanisms compared to other well-known methods: it acts more by indentation, digging into the aggregates surface and generating a new microtexture with, on average, less dense but taller and sharper peaks. Hard aggregates such as granites, greywackes and gneiss showed superior polishing resistance and better microtexture regeneration compared to softer materials like basalts, dolostones and limestones. The most influential properties were relative hardness (RHD), differential hardness (DH), mineral contents (quartz, feldspars, calcite), average mineral size (ϕm) and grain size distribution parameters (coefficient of variation CV and Gini-style index GSI), which showed the highest Pearson correlation coefficients with the final British Pendulum Number (BPNf). Predictive models developed with these properties achieved high accuracy (R^2 = 0.89 to 0.94), offering valuable tools for selecting aggregates with adequate skid resistance without performing polishing tests.

Introduction

Loss of skid resistance on road surfaces is a major safety concern, as it increases the risk of vehicle skidding and sliding, particularly under wet conditions[1]. In Quebec, nearly 29,000 individuals were involved in traffic accidents in 2022, with close to 400 fatalities reported[2]. Difficult road surface conditions, like wet pavement and aquaplaning, rank among the leading contributing factors, accounting for approximately 15.3% of reported accidents[3]. Numerous international studies have demonstrated strong correlations between accidents on wet roads and surface characteristics such as microtexture, macrotexture, rutting, and roughness[4]. The Quebec MTMD addresses this issue through the proper selection of coarse aggregates, based on their intrinsic and microtextural properties[5]. The latter, represented by the Coefficient of Polishing by Projection (CPP), are evaluated using the LC 21-102 test method. The test includes an accelerated polishing process via emery projection and the measurement of residual friction using the British pendulum[6]. However, recent observations of premature pavement wear, due to excessive polishing of coarse aggregates that initially passed the CPP test, have raised concerns about the accuracy of current evaluation parameters[7]. In this context, this study was launched to reassess critical components of the method, including polishing time and wear mechanisms.

Skid resistance characterization

Skid resistance refers to the ability of the tire-road interface to develop friction forces under dynamic conditions[8]. This property decreases over time due to traffic-induced polishing, which progressively alters the microtexture of the pavement surface[9,10]. Tourenq and Fourmaintraux[11] identified two principal mechanisms that govern this deterioration: *general polishing*, which results from uniform wear and depends mainly on the hardness of the aggregate, leading to peak rounding; and *differential polishing*, which develops from differences in mineral hardness (differential hardness) and helps maintain residual relief on the surface. The residual friction coefficient, closely linked to microtexture, is commonly used to assess skid resistance. It can be measured either in situ or in the laboratory. Laboratory procedures involve two steps: accelerated polishing of aggregates to simulate traffic wear, followed by measurement of the residual friction. Three main polishing methods are currently used: the pneumatic polishing, the Wehner and Schulze (W/S) machine and the polishing by projection. Widely adopted in Europe[12] and Australia[13], the pneumatic polishing method uses a rubber-tired wheel to polish specimens in the presence of water and abrasive (corn and flour). Residual friction is then assessed via the British pendulum, determining the Polished Stone Value (PSV). The W/S machine, commonly used in research, polishes circular specimens using rotating rubber cones and measures residual friction at high-speed using a second rotating head, equipped with rubber pads. It is supposed to offer a better simulation of real-world polishing effects[14]. The polishing by projection, mainly used in Quebec, accelerates both polishing and sample preparation, an advantage for the MTMD, which tests over 120 sources of quarried aggregates per year. It involves projecting fine emery and water at high pressure for about one hour, aiming to simulate the “limit polishing state” of aggregates under real traffic conditions[15]. This method was developed in France after studies revealed that, in the PSV test, 70 to 100% of the wear was induced solely by the abrasive, while the pneumatic-aggregate interaction plays a minor role. Accordingly, removing the pneumatic and only projecting the abrasive with a kinetic energy equivalent to the tire load will generate a similar polishing effect[16].

Development and limitations of the LC 21–102 polishing by projection method

Limited research has explored the impact of polishing by projection time on aggregate polishing resistance. The LC 21–102 polishing by projection method was originally developed by Delalande[16] in the 1990s and adapted for Quebec based on the work by Julien[17]. Since then, the protocol has remained largely unchanged. At the time, 20 cycles were considered sufficient to simulate maximum in-service wear, based on studies by Bédard[18] and Do et al. [19]. The results also correlated well with those from the PSV test[20]. However, these studies presented certain limitations. For instance, Bédard’s tests included a sandblasting step, potentially compromising aggregate surface integrity, while Do’s research involved only a small number of aggregate types. Moreover, since the 1990s, traffic volumes have increased[21,22], as has the use of studded tires[23] and winter abrasives[24], which has led to increased damage to the pavement surface layer. These changes suggest that a 20-cycle polishing may no longer be sufficient to replicate actual field conditions. Reports of premature wear in pavements, linked to over-polished aggregates that passed the CPP test, support this concern[7]. This study therefore re-evaluates key parameters of the LC 21-102 method, notably polishing time and wear mechanisms, to ensure laboratory results remain representative of real-world performance.

Effect of mineralogical and petrographic properties of the aggregates

The ability of an aggregate to retain its microtexture under traffic polishing depends on its mineral composition, general (also called relative) hardness, differential hardness and grain size[25,26] among other factors. Aggregates with high relative hardness tend to better retain their microtexture, as their

constituent minerals are more resistant. Additionally, aggregates with high differential hardness undergo uneven polishing due to the contrast in hardness among their mineral components, helping preserve surface microtexture[27,28,29]. Grain size also plays a key role. Studies by Wang et al.[30] show that finer-grained rocks have higher polishing resistance. Moreover, research by Roy and Kuna[31] suggests that a broader grain size distribution helps sustain microtexture by creating a more irregular, durable surface relief.

Objectives and scope of work

The primary objectives of the study are the following: to assess the effect of polishing time on aggregate polishing resistance; to determine whether the polishing limit state (or maximum wear) is reached within the 20 cycles prescribed by the LC 21–102 test method; to gain a better understanding of the wear mechanisms specific to polishing by projection (particularly through the evolution of microtexture parameters); to evaluate the influence of mineralogical and petrographic properties (such as mineral composition, grain size, general and differential hardness) and to predict the polishing resistance of aggregates. To attain these objectives, the experimental program was divided into two phases. The first phase involves four aggregates selected to investigate the effects of polishing time and mechanisms. Their friction and microtextural properties were measured before and at incremental stages of polishing (05), up to 40 cycles (twice the number of cycles prescribed by the LC 21–102) to monitor the evolution of the polishing resistance and microtexture. The second phase involves fourteen additional aggregates (for a total of eighteen); their friction and microtextural properties were determined before and after polishing to evaluate variations in polishing resistance across aggregate types (the selection of 35 cycles of polishing is based on the results from the first phase).
Several tests were conducted to determine the mineralogical, petrographic and mechanical properties of the selected aggregates. Mineral proportions, textures and grain sizes were determined through a combination of thin sections and quantitative X-ray diffraction (XRD; Rietveld method) analyses. Moreover, the mechanical properties of the aggregates were assessed using the micro-Deval (MD) and Los Angeles abrasion (LA) tests, following respectively the LC 21-070 and LC 21-400 test methods[32,33]. The conventional CPP at 20 cycles was also determined.

The Relative Hardness (RHD) and Differential Hardness (DH) values were calculated using Equations 1 and 2, based on the work of Tourenq and Fourmaintraux[11], updated by Kane et al.[14]:

$$\text{RHD} = \frac{1}{100}\sum_{i=1}^{n} p_i * h_i \qquad \text{Equation 1}$$

$$\text{DH} = \frac{1}{100}\sum_{i=1}^{n} p_i * \left|h_i - h_p\right| \qquad \text{Equation 2}$$

where i represents an identified mineral, n is the number of identified minerals in the aggregate, p_i is the proportion of each mineral (determined from quantitative XRD results), h_i is the Mohs hardness of each mineral (according to Klein *et al.* 2008[34]) and h_p is the Mohs hardness of the most abundant mineral in the aggregate.

Several petrographic properties were assessed for the selected aggregates. First, the weighted average mineral size (ϕm) represents the mean grain size of the minerals composing the aggregate, weighted by their surface proportion. It was determined using Equation 3:

$$\Phi\text{m} = \sum_{i=1}^{n} p_i * \varphi_i \qquad \text{Equation 3}$$

where p_i is the surface proportion and φ_i is the average size of each identified mineral (both estimated from the thin sections analyses).
Secondly, the grain size distribution was estimated using the standard deviation σ and the coefficient of variation (CV), determined with Equations 4 and 5. They measure, respectively, the absolute and relative

dispersions of grain sizes around the mean φ_m. Higher values of σ and CV indicate greater variation in grain size distribution.

$$\sigma = \sqrt{\frac{1}{n}\ \sum_{i=1}^{n}(\varphi_i\ -\varphi_m)^2} \quad \text{Equation 4}$$

$$CV = \frac{\sigma}{\varphi_m} \quad \text{Equation 5}$$

A Gini-style Index (GSI) was also calculated to estimate the grain size distribution, following Equation 6 proposed by Brown (1994)[35]. While traditionally used in economics to assess income distribution inequality, GSI can be adapted to other fields. The index ranges between 0 and 1: values close to 1 indicate a highly heterogeneous grain size distribution while values close to 0 indicate a more homogeneous grain size distribution.

$$GSI = 1 - \sum_{i=0}^{n-1}(Y_{i+1} + Y_i) * (X_{i+1} - X_i) \quad \text{Equation 6}$$

where Y_i represents the cumulative proportion of average mineral sizes for the *n* identified minerals, X_i is the cumulative proportion of the surface percentages of the minerals. The mineral sizes are arranged in ascending order from the smallest to the largest.

Materials and methods

Materials

The eighteen (18) aggregates selected for this study are commonly used in road and highway construction across the province of Quebec. These include nine sedimentary rocks (two greywackes-Gwk1/Gwk2, two dolostones-Dol1/Dol2, five limestones-Lim1 to Lim5), eight igneous rocks (six granites-Gra1 to Gra6, two basalts-Bas1/Bas2), and one metamorphic rock (gneiss-Gns). The four aggregates used in the first phase are Gra2 (reference aggregate), Gra3, Bas2 and Dol2. The selection represents the main geological regions in the province of Quebec and exhibits a broad diversity in key parameters: polishing resistance (BPN), mineralogy (composition, RHD, DH), average mineral grain size (ϕm), physical and mechanical properties (LA, MD).

Greywackes (Gwk) are characterized by a fine-grained (<100 µm) matrix of relatively soft minerals (clay minerals, micas), interspersed with harder and coarser minerals, including quartz (34-43 %), feldspars (21-34 %), and calcite (1.5-2.0 %). Grains exhibit a generally sub-rounded morphology with few sharp edges. Gwk1 has a finer grain size (ϕm = 145 µm) and a higher variation in crystal sizes (higher CV, GSI) compared to Gwk2 (ϕm= 203 µm) and possesses a higher RHD but a lower DH (Table 1).

The granites (Gra) and granitic gneiss (Gns) primarily consist of hard minerals such as quartz (16.4 % on average), feldspars (46.6 %), pyroxenes (7.5 %) and amphiboles (4.1 %), giving them high RHD ranging from 4.30 to 5.30. They also contain smaller amounts of soft or carbonate minerals, such as micas (4.3 %), calcite (0.6 %) and dolomite (0.3 %). The presence of minerals with varying hardnesses results in diverse DH, ranging from 0.88 for Gra2 to 0.23 for Gra5 (Table 1). Granitic gneiss (Gns) is distinguished by a foliated or banded texture, alternating between light-colored layers rich in quartz and feldspars, and darker layers enriched with micas and amphiboles (hornblendes). This rock group is coarser-grained than the others, with ϕm values ranging from 300 µm to 860 µm. The grain size distribution varies significantly with CV and GSI ranging, respectively, from 0.44 to 0.59 and 0.32 to 0.90.

Basalts (Bas) are fine-grained volcanic rocks, with matrices primarily composed of feldspars (from 18.4 % for Bas1 to 36.3 % for Bas2), pyroxenes (16.5 to 19.8 %, sometimes altered), and micas (13.8 %). Bas1 contains quartz veins (7.5 %) traversing its matrix, whereas Bas2 is characterised by calcite (6.7 %) and chlorite (13.8 %) amygdules, reaching up to 600 µm in diameter. Basalts are finer-grained than granitic rocks, with ϕm values of 222 µm for Bas1 and 212 µm for Bas2. Their grain size distribution parameters (CV, GSI) display moderate values, reflecting a relatively homogeneous granulometry. While basalts have

lower RHD than granites, they exhibit higher DH on average, attributed to the diversity of mineral hardness (Table 1).

Dolostones (Dol) consisted predominantly of dolomite (>70 %), with clay minerals (<5 %) dispersed within the matrix or in veins. Arkose veins, composed of quartz (3.7 %) and feldspars (13.7 %), are present in Dol1. Dolostones are fine-grained (ϕm < 120 µm) and have relatively homogeneous mineral sizes, as indicated by moderate CV, σ and GSI values. They also have lower RHD than greywackes and igneous rocks but exhibit higher DH (0.48 and 0.51 on average) (Table 1).

Limestones (Lim) are primarily composed of calcite, with variations mainly in grain sizes between samples. In Lim1, Lim4 and Lim5, the matrix consists predominantly of fine to medium grained calcite (30–800 µm), whereas in Lim2 and Lim3, the calcite is micritic (<10 µm on average). Clay minerals are present in veins or dispersed throughout the matrix. Some limestones, such as Lim4 and Lim5, are largely monomineralic. Additionally, dolomite crystals (9.9 % on average), micas (3.0 %), quartz (4.9 %), and feldspars (3.8 %) are present in the matrix. Grain size varies within this group: Lim1, Lim4, and Lim5 are medium-grained (ϕm= 300-490 µm) while Lim2 and Lim3 are very fine-grained (ϕm=66 µm and 29 µm, respectively). This variation is reflected in the CV, which are higher for Lim2 and Lim3. Limestones represent the group with the lowest hardness values, with RHD ranging from 2.70 to 3.50. DH values are also low (0.20-0.64), except for Lim1, which exhibits a DH of 0.96 (Table 1).

Table 1. Mineralogical, petrographic, and mechanical properties determined with XRD and thin sections analyses for the selected aggregates.

Id	RHD	DH	Qz	Pl	Cal	Dol	ϕm	σ	CV	GSI	CPP	LA	MD
Units	-	-	%	%	%	%	µm	µm	-	-	-	%	%
Gwk1	5.30	0.81	43.0	19.5	2.0	-	145.4	83.4	0.55	0.79	0.54	8	17
Gwk2	4.10	1.33	34.4	19.3	1.5	-	203.0	122.3	0.50	0.43	0.53	11	17
Gra1	5.10	0.45	17.4	33.5	0.3	0.2	723.2	336.3	0.44	0.32	0.54	7	27
Gra2	5.30	0.88	28.5	27.8	8.0	-	294.4	162.4	0.55	0.55	0.55	6	15
Gra3	5.10	0.49	27.4	30.1	0.4	-	856.0	455.5	0.55	0.56	0.53	12	33
Gra4	4.80	0.30	11.9	43.7	0.8	0.5	558.7	268.5	0.47	0.57	0.52	12	26
Gra5	4.30	0.23	4.3	45.7	0.7	1.0	567.9	324.7	0.57	0.36	0.50	5	18
Gra6	5.20	0.40	22.6	23.6	2.5	0.3	441.3	244.4	0.59	0.90	0.51	5	21
Gns1	5.40	0.35	18.1	33.1	0.4	0.5	466.0	213.6	0.46	0.47	0.50	6	26
Bas1	4.10	0.32	7.5	18.4	-	-	221.7	112.3	0.50	0.45	0.50	4	7
Bas2	4.60	0.85	1.7	36.3	6.7	-	211.6	158.3	0.68	0.74	0.49	8	13
Dol1	4.00	0.51	3.7	0.5	1.0	72.7	115.9	69.5	0.58	0.45	0.52	6	20
Dol2	3.50	0.96	4.7	0.7	0.9	74.7	377.6	73.3	0.62	0.69	0.45	4	17
Lim1	3.10	0.64	8.8	0.0	49.8	8.7	66.1	172.1	1.15	0.59	0.43	6	21
Lim2	3.90	0.48	5.7	2.3	50.8	19.0	103.9	68.3	0.61	0.94	0.47	13	22
Lim3	2.70	0.30	3.6	0.0	62.5	10.4	29.0	43.1	1.54	0.68	0.45	11	22
Lim4	2.80	0.23	2.2	0.0	70.2	8.5	489.4	385.0	0.79	0.75	0.42	14	31
Lim5	3.00	0.20	4.3	0.4	86.1	2.7	308.9	172.8	0.49	0.91	0.39	9	25

Specimen preparation and changes to the conventional procedure

The specimens used in the LC 21-102 test consist of flat, rectangular particle mounts measuring 90 mm x 100 mm. Three specimens were prepared for each selected aggregate to be paired with a reference aggregate specimen. The specimens are made using cubic-shaped particles, with dimensions ranging from 7.2 mm to 10 mm. The conventional preparation procedure, as described in the LC 21-102 test method, comprises three main steps. First, the particles are placed at the bottom of an ultra-high molecular weight (UHMW) polyethylene mold by vibration. Next, a layer of plaster is poured to immobilize the particles in place. Finally, the mold is filled with epoxy resin, which forms the base of the specimen. After several hours of curing, the specimens are demolded. At this stage, the aggregate particles are entirely covered by plaster, which is then removed by brushing under water to expose the «clean» aggregate surface, ready for pendulum testing. However, during the preliminary testing phase, the presence of residual plaster was identified through micro X-ray fluorescence (µXRF) analysis on the specimen surface. Stoichiometric analyses, primarily aimed at confirming the mineral phases of quartz-based grains (91.55%), revealed elevated levels of sulfur (6.14%) and calcium oxide (1.71%) (two key components of plaster). These elements were found within quartz-rich zones, indicating contamination of the aggregate surface. Figure 1 indeed reveal that plaster residues are widely distributed across the entire specimen surface prepared with the reference aggregate.

Figure 1. Distribution map of sulfur (S) and calcium (Ca) on the particles of the reference aggregate specimen after polishing, highlighting the presence of plaster residues across the particle surfaces. Map was generated using a µXRF instrument (Bruker M4 Tornado) equipped with a Rhodium (Rh) tube operating at 50 kV and 600 µA, producing a beam with a 40 µm diameter.

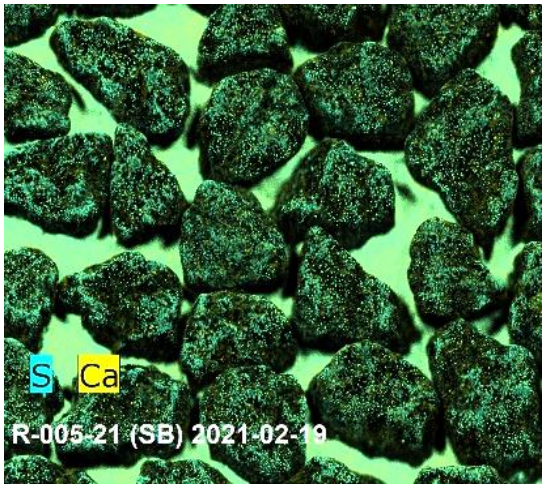

The presence of residual plaster on the aggregate particle is considered to have a negligible impact on the results of the British Pendulum Test. However, it could affect the accuracy of the microtexture analyses conducted in the study. Indeed, SEM micrographs, presented at Figure 2, revealed gypsum crystals of considerable size (reaching several tens of microns) embedded within the surface relief. As microtexture is defined by peaks below 500 µm horizontally and 200 µm vertically, the presence of such crystals within the peaks could interfere with the surface measurements obtained via 3D microprofilometry, both before and after polishing. To avoid these interferences, several mechanical and chemical cleaning methods were applied to conventionally fabricated specimens. These included mechanical brushing, compressed air jets, and chemical treatments using solvents like ethanol and xylene. However, these methods were ineffective

to completely eliminate the plaster residues from the aggregate surfaces. Consequently, an alternative procedure of specimen fabrication was developed. This new protocol replaces the initial layer of plaster with clean sand, inspired by existing standards such as EN 1097-8 and the retired French standard XP P18-580, where sand is already used in specimen mounting. The modified preparation consists of three distinct layers: a first «protective» layer of sand (at the bottom of the mold and between the coarse aggregate particles), composed of clean grains sized between 500 and 630 µm (coarser than microtexture); a second impermeabilizing layer consisting of a mixture of quick-setting resin and aluminum oxide; and a third and final layer of epoxy resin. The coarse nature of the sand protection layer prevents it from embedding in the microtexture of the particles, thereby avoiding any deleterious impact on the microprofilometer analyses. The impermeabilizing layer prevents the third layer of resin from percolating and reaching the surface of the particles. This ensures that the surface of the particles remains clean and clear of any type of residues (plaster or resin) for further analyses. Figure 3 presents a summary of the modified specimen preparation procedure.

Figure 2. Scanning electron microscope (SEM) micrographs of specimen after polishing, highlighting the presence of plaster residues in the forms of gypsum crystals between (mineral) grains of aggregate particles. Analyses were conducted with 4 µm beam size, a voltage between 15 to 20 kV and magnifications of 700 times.

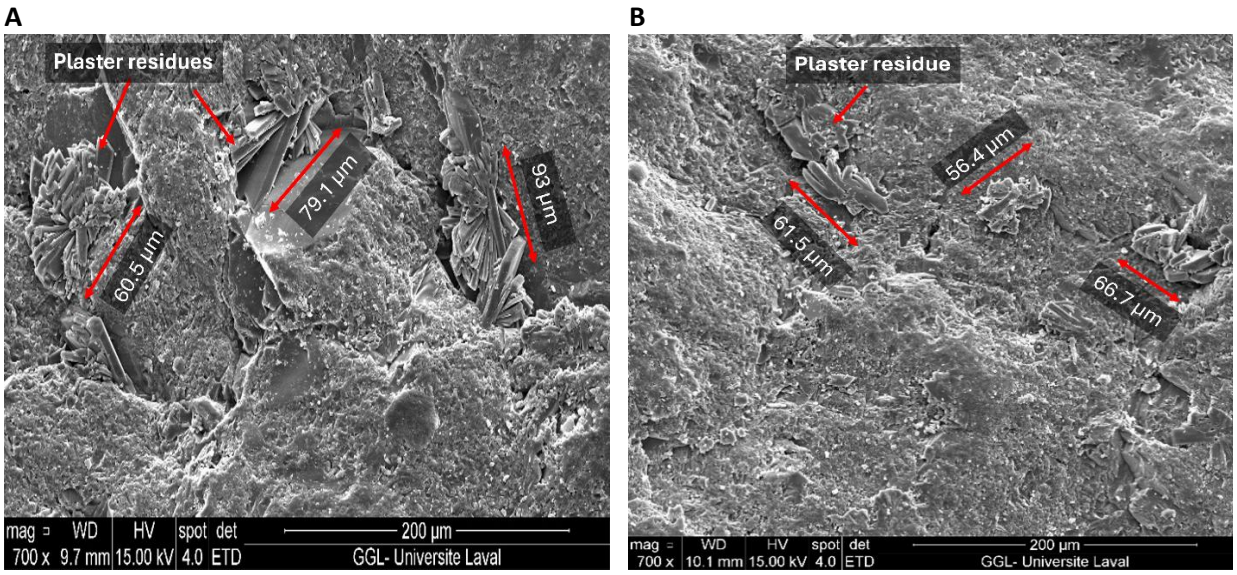

Polishing and friction measurement devices

Four specimens are polished simultaneously in the projection machine (Figure 4), in accordance with the LC 21-102 test method, comprising one reference aggregate and three from different sources (Figure 4.A). They are subjected to a high-pressure stream of water (10 MPa) containing fine abrasive particles of aluminum oxide. This mixture is directed through a 40-degree inclined nozzle, positioned 20 cm away from the specimens, with a water flow of 600 l/h and an abrasive flow of 500 g/min. The nozzle moves back and forth along a plane parallel to the specimens surfaces, at a speed of 105 ± 5 mm/s (Figure 4.B). After polishing, the specimens are submerged in water for 30 minutes before undergoing the British pendulum test.

The British pendulum is defined by the EN 13036-4 standard[36] (Figure 5). It consists of a spring-loaded 76.2 mm × 25.4 mm slider, made of standardized rubber, attached to the end of the pendulum arm. Ten

pendulum releases are done for each specimen, and the BPN are noted. The CPP value is then assessed with the average BPN according to Equation 7.

Figure 3. Specimen preparation procedure illustrating: A) the disposal of individual coarse aggregate particles at the bottom of the mold; B) the first layer of sand spread at the bottom of the mold between the coarse aggregate particles; C) the installation of the second layer (quick-setting epoxy and aluminum oxide) using an icing nozzle, and D) the final specimen with a clean surface for the British pendulum test.

Figure 4. Polishing resistance test setup in accordance with LC 21-102: A) polishing machine showing the inclined nozzle projecting abrasive onto the specimens placed on the holder, and B) polishing process of test specimens illustrating the inclined nozzle moving along the arrow-indicated path to project abrasive on the specimens during a single polishing cycle.

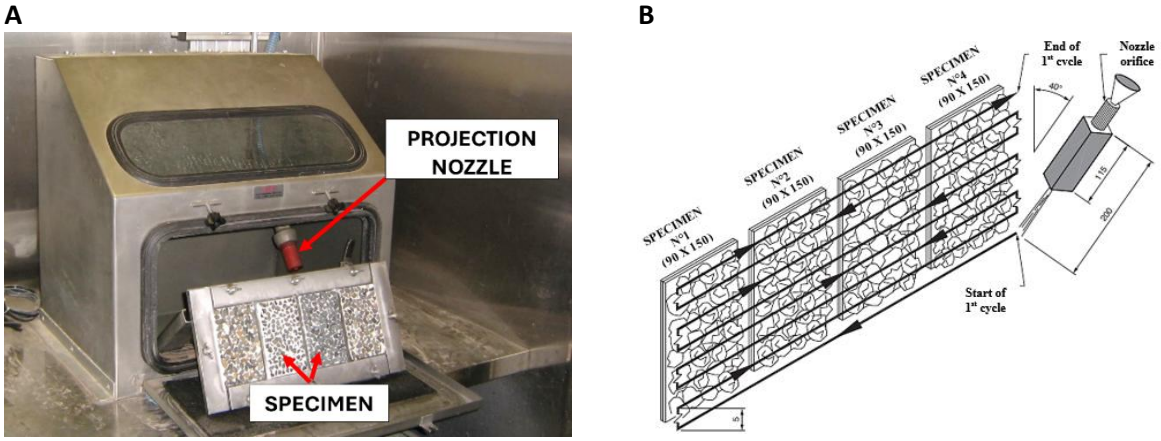

Figure 5. Friction measurement device: A) British pendulum; B) rubber slider on the specimen.

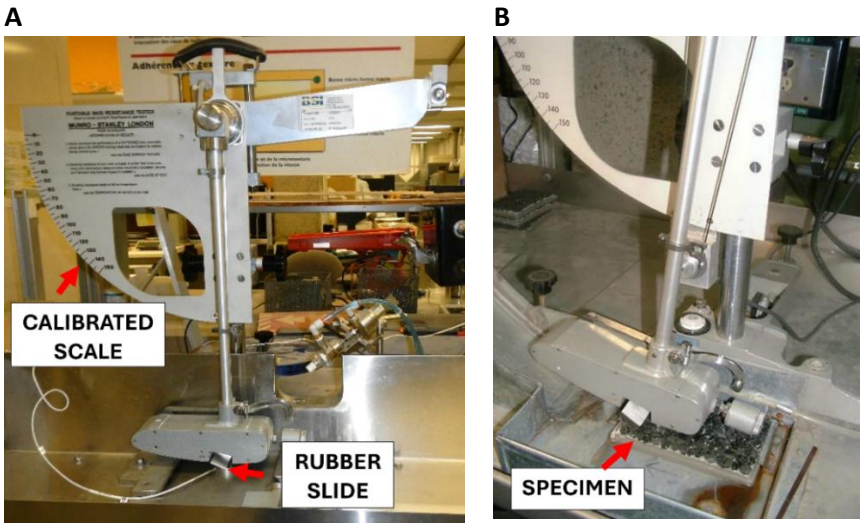

$$CPPi = \frac{\overline{BPN_E} - \overline{BPN_R} + 55.3}{100} \quad \text{Equation 7}$$

where CPPi is the individual result of the tested specimen (%); $\overline{BPN_E}$ is the mean raw result of the 10 releases of each tested specimen; $\overline{BPN_R}$ is the mean result for the 10 releases of the reference specimen polished simultaneously with the tested specimens; and 55.3 is the expected BPN value of the reference at 20 cycles.

Microtexture characterization and parameters

The microtexture measurements were conducted using a 3D laser microprofilometer (Gocator 2520 by LMI Technologies-Figure 6). Details about the device are available at Kandji et al. (2025)[37]. The specimens are arranged on a mobile scanning stage (Hydra V-741 by PI USA). The analyses were performed at a 7.5 µm resolution (in the X and Y directions), at exposure times between 50 µs and 75 µs. The data are analysed with the *MicroAnalysis 1.1* software, developed by the MTMD. It enables the differentiation between macrotexture and microtexture data by applying wavelength filters. The microtexture is obtained by extracting wavelengths below 500 µm. The microtexture is then characterized by various parameters describing the peaks composing the microtexture in terms of density (N_p), shape (α) and size (height H, gradient Grad_H, average positive height sH). They were determined through replication of the indentor technique and proven to be good indicators of the microtexture evolution under polishing[37]. The N_p parameter is determined by electronically counting the number of peaks on the particle surface and dividing it by their total surface area. The shape parameter is expressed as the cotangent of the peak semi-angle (α). The Grad_H parameter quantifies the absolute height difference between consecutive peaks. The *surf_height* (sH) parameter represents the average height of peaks above the mean height of the particle. These parameters are calculated for profiles in both X and Y directions, and their average value is subsequently determined (except for the sH parameter). The equations used to calculate the parameters, and their graphical representation are presented in Table 2.

Figure 6. Microtexture measurement device with A) four specimens placed on the stationary scanning stage and B) the 3D laser microprofilometer, model: Gocator 2520 scanning a specimen on the moving scanning stage.

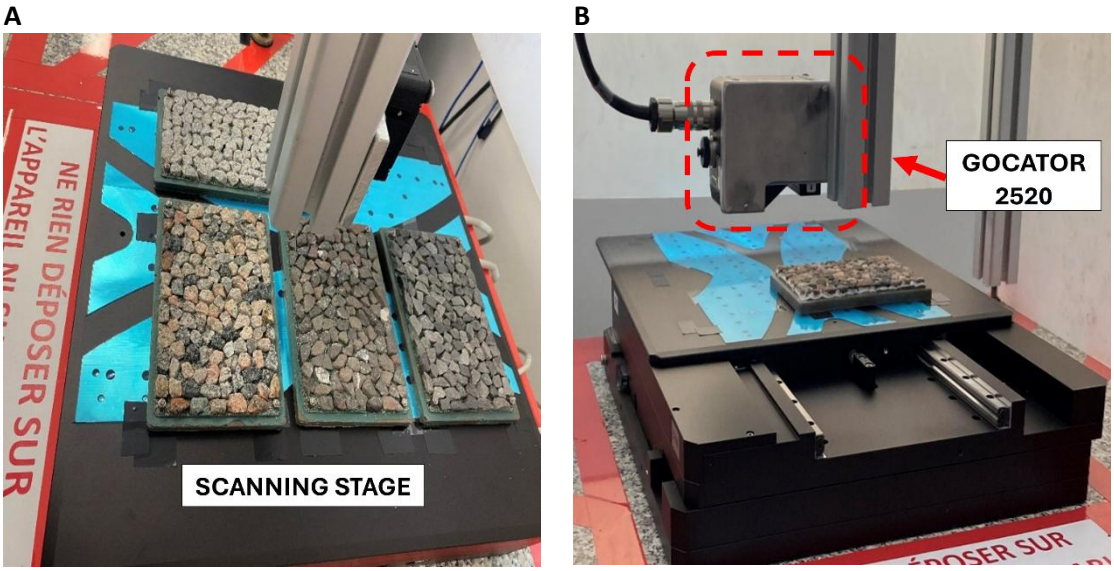

Table 2 : Equations used to calculate the microtexture parameters and their graphical representations.

Parameters		Units	Equations	Graphical representations
Density	Peak density (Np)	-	$Np = \frac{\text{Total count of peaks}}{\text{Total particle surface}}$	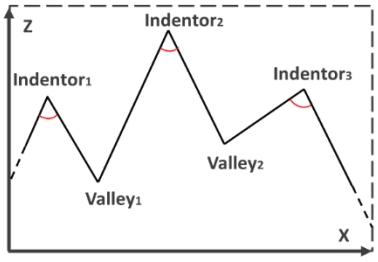
Height	Peak height H	mm	$H_2 = \frac{(Z_{I2} - Z_{V1}) + (Z_{I2} - Z_{V2})}{2}$	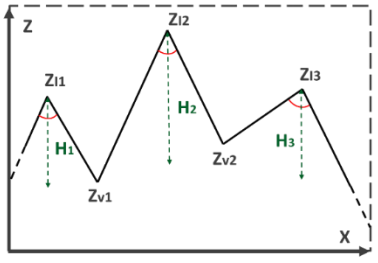
Shape	α	(°)	$\alpha_2 = \frac{1}{2} \times \left[tan^{-1} \left\lvert \frac{X_{I2} - X_{V1}}{X_{I2} - X_{V1}} \right\rvert + tan^{-1} \left\lvert \frac{X_{V2} - X_{I2}}{X_{V2} - X_{I2}} \right\rvert \right]$	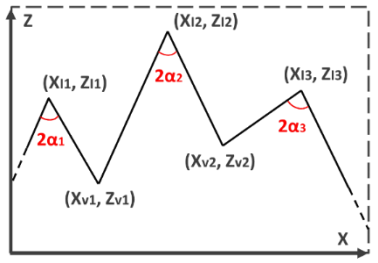

Scanning electron microscope (SEM)

Scanning electron microscope (SEM) analyses were conducted on polished (40 cycles) and unpolished particles. The polished particles were cut from the polished specimens to dimensions of approximately 4 cm by 4 cm, to fit the SEM sample chamber. The unpolished particles were selected from the same facies as the polished particles, before being made into small specimens (4 cm by 2 cm). Once cut or made, the polished and unpolished pieces were coated with a thin layer of carbon to make their surface conductive, enabling observations of texture and semi-quantitative analyses. The analyses were conducted with a FEI Inspect F50 model, at a voltage of 15 kV and magnifications ranging from 75 and 900 times.

Results and discussion

Effect of polishing time and aggregates maximal wear

Figure 7 presents the evolution of average (based on three specimens) and absolute values of BPN over successive polishing cycles, obtained in the first phase of testing. Figure 7.A shows a consistent decrease in BPN for the four aggregates, all following a similar trend. Gra2 had the highest BPN at 0, 20 and 40 cycles, followed by Gra3, Bas2, and Dol2. The sharpest decline occurred during the first 15 cycles: from -16.6% for Dol2 to -8.3% for Gra2. Notably, Gra2 showed a slight rebound between cycles 5 and 10 (+0.3%), which could be due to the replacement of the slider following excessive wear. Between cycles 15 and 25, the decrease in BPN continued, but at a slower rate: from -4.8% for Dol2 to -4.1% for Gra2. From cycle 25 to 40, BPN for Dol2 stabilized at 46.2, while Bas2, Gra3 and Gra2 exhibited only minor additional losses (-1,1% to -1.7%), reaching stable values near the 35th cycle. Results at 40 cycles confirmed this stabilization, with no significant changes after. Figure 7.B shows that Dol underwent the most substantial overall decrease, followed by Bas2. Gra2 and Gra3 demonstrated better resistance to polishing. Although Gra2 maintained the highest BPN values throughout the test, Gra3 experienced slightly less proportional loss (-13.0% for Gra3 and -13.9% for Gra2), indicating strong overall performance. These results suggest that the microtexture deterioration of aggregates continues beyond the 20-cycle threshold defined by the LC 21-102 test method. This potentially challenges the assumption that this polishing duration brings aggregate to their maximum polishing state or wear. Instead, the critical number of cycles required to reach maximum wear appears to be approximately 25 cycles for Dol2 and around 35 cycles for the other aggregates (Figure 7.B). This observation aligns with previous findings in the literature, where polishing tests generally reveal a stabilization point beyond which friction values plateau, indicating that the maximum wear condition has been reached[28,38,39].

This analysis is further confirmed by the results from the second phase of testing, conducted on all 18 aggregates. Figure 8 presents the BPN values measured at 0 (BPN_0), 20 (BPN_20), and 35 (BPN_35 or BPNf) polishing cycles. A clear decreasing trend in BPN with increasing polishing time is observed. Notably, the BPN at 35 cycles is consistently lower than at 20 cycles for most aggregates, except for Gwk2, Lim1, and Lim5, which exhibited slight increases of 0.4%, 5.6%, and 2.4%, respectively. These results reinforce the idea that the standard 20-cycle polishing duration may be insufficient to reach the maximum wear state of most aggregates when subjected to polishing by projection. Additionally, greywackes, granites, gneiss and basalts generally exhibit higher initial and post-polishing BPN values. In contrast, dolostones and limestones, particularly Lim1 and Lim2, have comparable initial BPN values but experience a greater decrease after polishing compared to other aggregates.

Figure 7. Evolution of average (based on three specimens) (a) absolute and (b) relative BPN over successive polishing cycles.

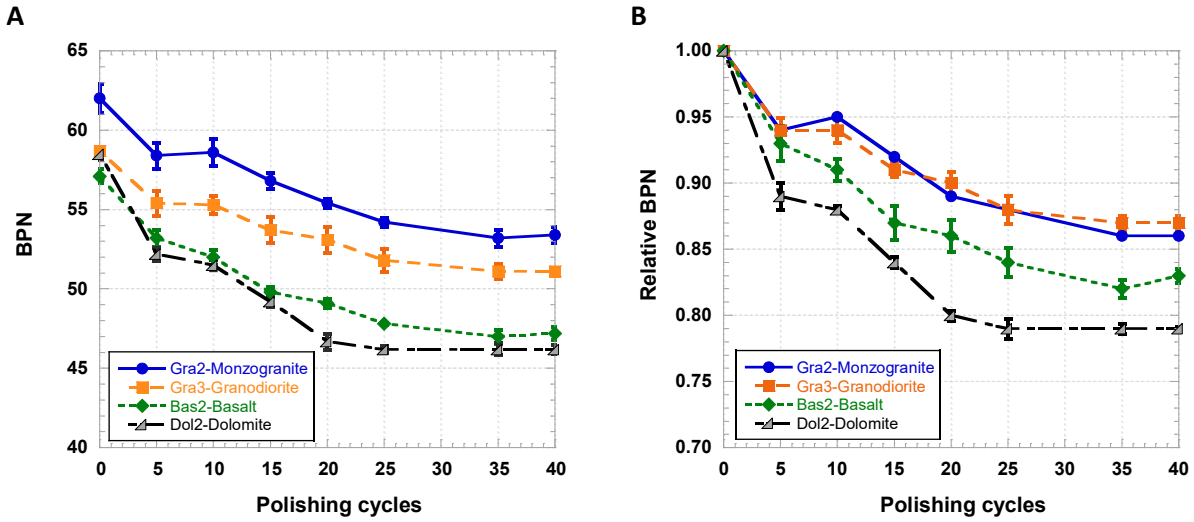

Figure 8. Evolution of average BPN values before (BPN_0 in green) and after 20 cycles (BPN_20 in grey) and 35 cycles (BPN_35 or BPNf for *final* in red) of polishing.

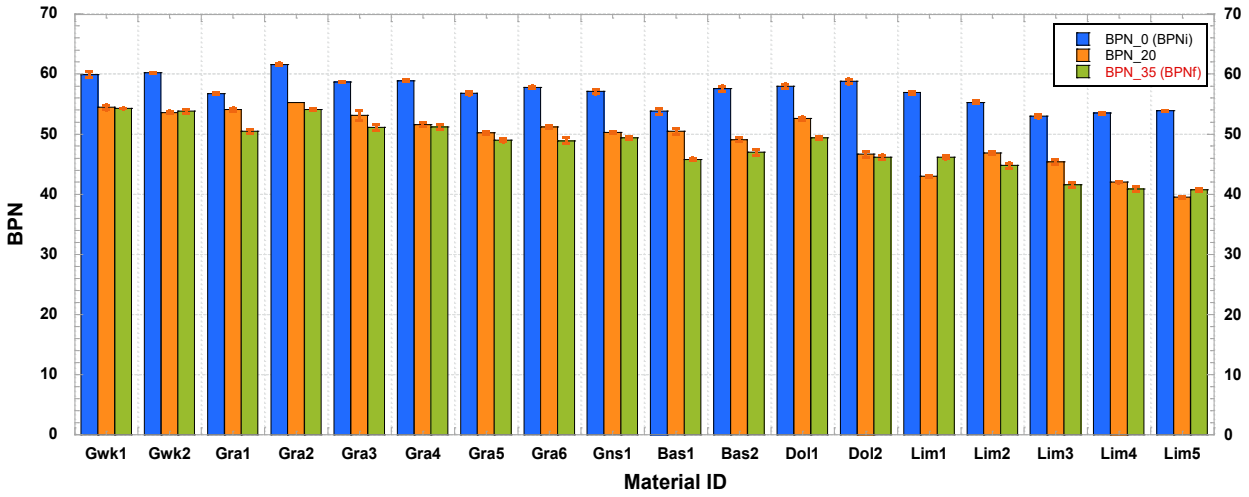

Evolution of microtexture, polishing mechanisms and phases of wear

Figure 9 presents the evolution of microtexture parameters over successive polishing cycles during the first phase of testing. Before and after polishing, Gra2 and Gra3 exhibit the lowest peak density (Figures 9.A, 9.B) and shape α (Figure 9.E) values, but the highest peak heights H (Figure 9.C). This indicates that their surface relief is initially composed of taller and sharper peaks, a characteristic that remains visible even after polishing. The most significant damage occurs between 0 and 5 cycles (Figure 7.B), representing a phase of accelerated wear marked by significant variations in microtexture. Peak height H (Figure 9.C) and shape α (Figure 9.E) increase, while peak density Np (Figure 9.A) decreases across all four aggregates. These effects are most pronounced for Gra2 and Gra3, confirming their distinct surface response compared to Bas2 and Dol2. These observations are consistent with findings by Do et al.[19], who reported that the most significant changes in peak count, shape and relief occurred within the first five polishing

cycles. Between 5 and 10 or 15 cycles, the damage slows down (Figure 7.B), corresponding to a deceleration phase. BPN continue to decrease, while peak density shows signs of recovery, particularly for Gra2 and Gra3 (Figure 9.B), suggesting the formation of new peaks. From 10-15 to 30 cycles, more fluctuations are observed in all parameters, indicating a dynamic phase of surface evolution. In terms of peak height H, two distinct behaviors emerge: Gra2 and Bas2 maintain relatively stable values (average variation < -1%), while Gra3 and Dol2 experience higher deterioration (Figure 9.D), with decreases ranging from -6% to -10% for Dol2, and -9% to -11% for Gra3. These trends persist up to 40 cycles, despite a slight rebound for Dol2. Between 30 and 40 cycles, the damage appears to stabilize. BPN values plateau (Figure 7.B), while peak height and shape show minimal variations. Additionally, a slight increase in peak density is observed for all aggregates, suggesting a steady-state surface condition. This three-phase segmentation of polishing-induced microtexture evolution (acceleration, slow down, stabilization) is similar to the model proposed by Guan et al.[9] for vertical wheel polishing.

According to the previous analysis, the polishing by projection mechanism can be described as follows. Initially (first five cycles), all aggregates experience general polishing, but aggregates with high RHD (Gra2 and Gra3) lose less peaks and retain more texture due to their mineral composition and hardness, while softer ones (Bas2 and Dol2) lose more peaks. In subsequent cycles (5 to 40 cycles), the projected abrasive "digs" the surface of the aggregates and sharpens them, making the remaining hard mineral peaks taller. Over time, the texture of low DH aggregates (Gra3 and Dol2) flattens, whereas high DH ones (Gra2 and Bas2) undergo differential polishing, regenerating microtexture and sustaining the roughness of their surface. This "digging" mechanism, which may sound counterintuitive for a polishing mechanism, was confirmed by SEM micrographs presented at Figures 10. They show textures of representative Gra2 and Dol2 particles, before and after polishing. It shows that Gra2 has a more pronounced surface texture compared to Dol2, due to the removal of soft minerals like biotite (Bt) and chlorite (Chl) (illustrated in Figures 10.A and 10.B), which are more sensitive to the polishing. The remaining peaks of quartz-Qz, plagioclase-Pl and alkali feldspaths-Kfsp, less sensitive to polishing due to their high hardness, became taller in contrast. In the case of Dol2, Figures 10.C and 10.D show that the dolomite-Dol and illite-Ill crystals, which dominate the surface and have low and similar hardness, are polished uniformly, which create a flatter texture.

Also, a comparison between polishing by projection and the other two polishing methods reveals notable similarities and differences in the microtexture evolution. Polishing by projection shares some effects with pneumatic and W/S methods, such as reducing peak density through the removal of soft minerals[9,40]. However, unlike projection, the latter two methods also reduce peak height and gradient, especially in soft aggregates like limestone[14,28,41,42]. This is due to the compressive (due to the weight of the device during contact) and abrasive forces that round and crush the peaks. However, for hard aggregates with high differential hardness such as greywackes, differential polishing leads to increased peak sharpness and height [9,28,38].

Figure 9. Evolution of average absolute (A, C and E) and relative (B, D and F) microtexture parameters over successive polishing cycles (Np = peak density; H = peak height; α = peak shape).

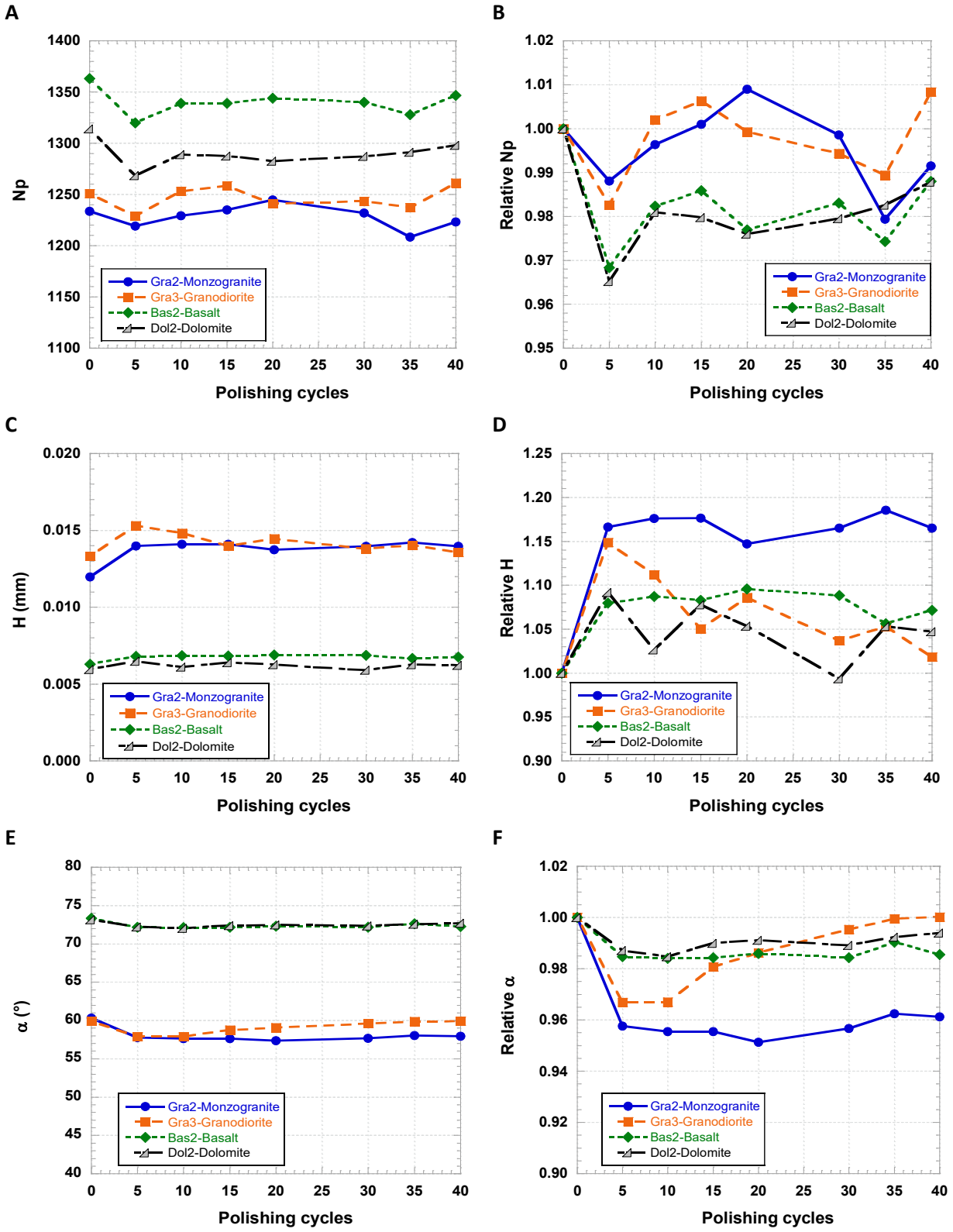

Figure 10. Scanning Electron Microscope (SEM) micrographs of the surface of representative particles of Gra2 and Dol2 before (A and C) and after (B and D) 40 cycles of polishing, highlighting the polishing mechanisms: Gra2 (A and B) experienced differential polishing with the digging of the surface where the abrasive projection selectively removes the softer minerals (Chl-chlorite and Bt-biotite), while the harder minerals (Qz-quartz, Pl-plagioclases, Kfsp-alkali feldspars) resist more effectively; Dol2 (C and D) experienced a more general polishing due to the abrasive projection digging and removing at a more uniform rate the soft minerals covering most of the surface (Dol-dolomite, Ill-illite).

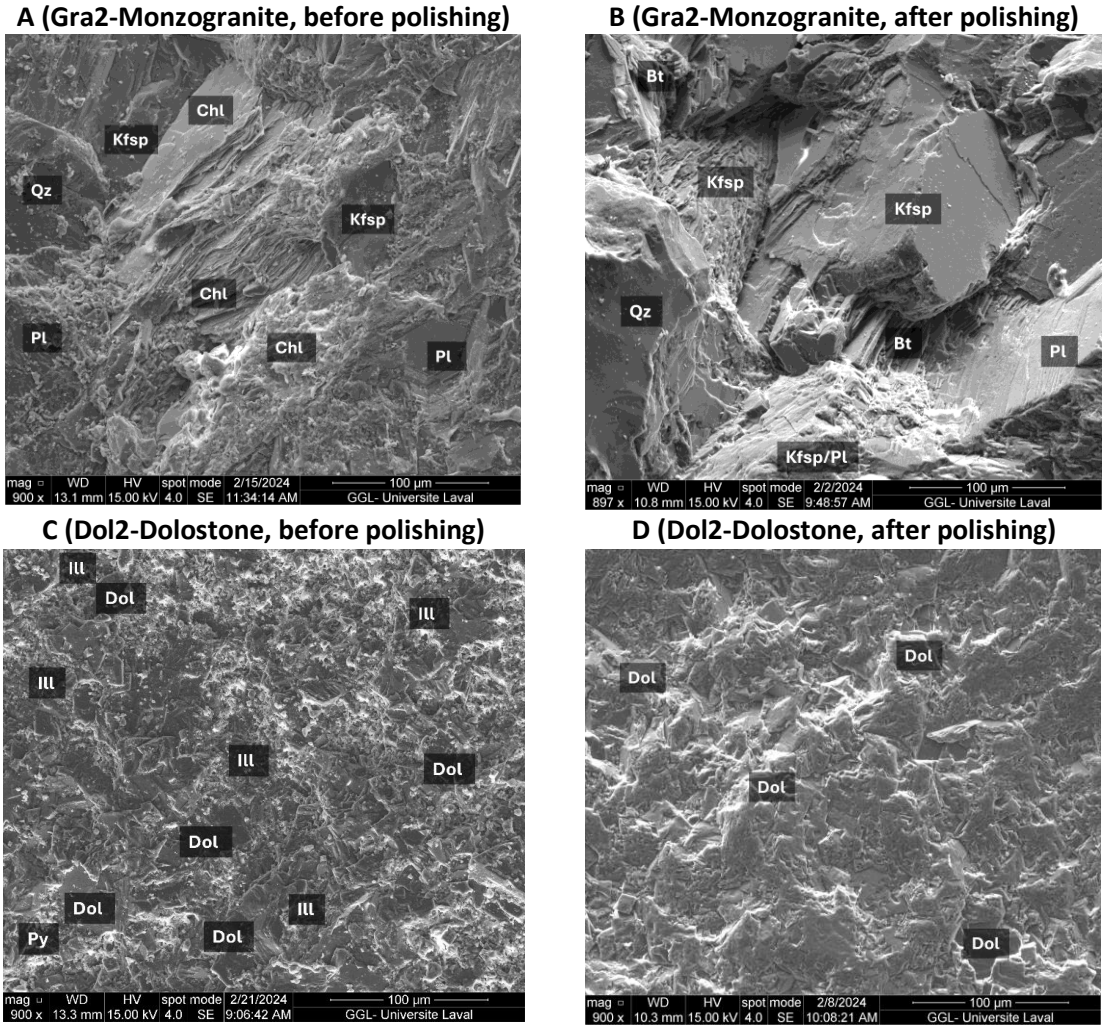

Effect of aggregates intrinsic and microtextural properties on polishing resistance

The first phase of the study suggests that intrinsic properties, particularly RHD and DH, strongly influence aggregate polishing resistance. This trend is confirmed in the second phase, where Pearson correlations (r) link both the BPNf (after 35 polishing cycles) and its variation ΔBPN (between 0 and 35 cycles) to aggregates properties (Table 3). RHD indeed shows the highest positive correlation, followed by the contents of hard minerals like quartz (Qz) and plagioclase (Pl). Soft minerals like calcite (Cal) and dolomite (Dol) show negative correlations. DH also contributes positively, though to a lesser extent. It means that aggregates with high RHD, DH and proportions of hard minerals (greywackes, granites, gneiss), and conversely low proportions of soft minerals demonstrate the best performance. SEM micrographs (Figure

11) of Gra2, Gra3, Bas2, and Dol2 illustrate their textural differences, tied to these variables, highlighting the hard aggregates (Gra2 and Gra3, with high RHD and high hard mineral contents) having a more textured surface than soft aggregates after polishing.

Table 3. Pearson correlation coefficients (r) between BPNf / ΔBPN and most influential mineralogical and petrographic properties of the selected aggregates.

	RHD	DH	Qz	Pl	Cal	Dol	ϕm	σ	CV	GSI
BPNf	0.833	0.528	0.796	0.609	-0.820	-0.155	0.231	0.088	-0.538	-0.417
ΔBPN	0.814	0.377	0.751	0.670	-0.807	-0.294	0.308	0.147	-0.495	-0.611

Figure 11. Scanning Electron Microscope (SEM) micrographs of the surface of representative particles of the dominant facies of various aggregates, after 40 cycles of polishing, highlighting the effect of RHD: Gra2 (A) and Gra3 (B) with high RHD present visibly more textured surfaces with deeper valley and higher peaks, contrasting with Bas2 (C) and Dol2 (D), with low RHD, which present less textured surfaces.

A (Gra2-Monzogranite:
RHD=5.30, DH=0.88, Qz=28.5%, Cal=0.0%)

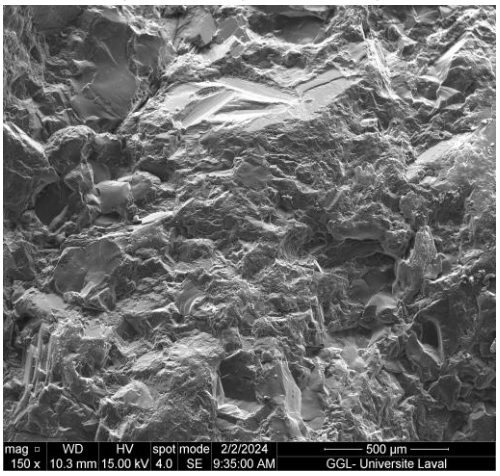

B (Gra3-Fine-grained granodiorite:
RHD=5.10, DH=0.49, Qz=27.4%, Cal=0.4%)

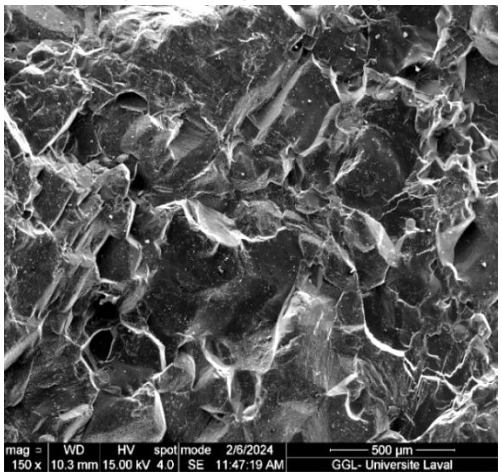

C (Bas2-Massive basalt:
RHD=4.65, DH=0.85, Qz=1.7%, Cal=6.7%)

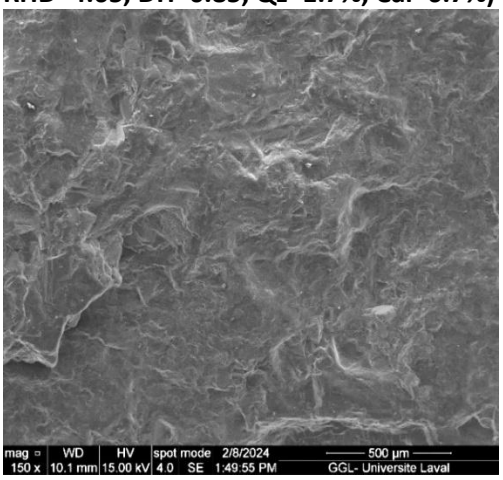

D (Dol2-Cristalline dolostone:
RHD=3.91, 0.48, Qz=4.7%, Cal=0.9%)

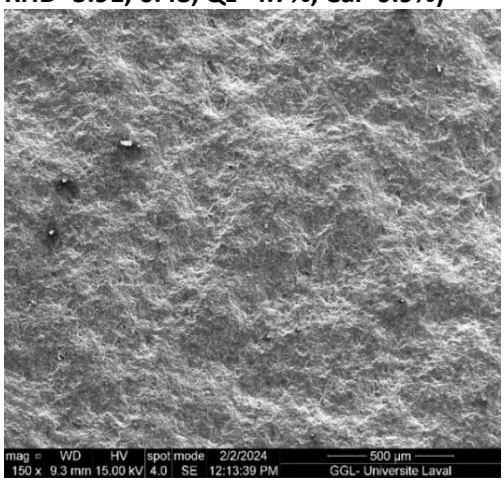

Grain size distribution properties such as σ, GSI and CV show no significant, or negative correlations, with BPNf and ΔBPN (Table 3), suggesting that uniform grain structures enhance polishing resistance. Additionally, the mean grain size (ϕm) shows no significant correlation ($r < 0.310$). These results seem to contradict those of earlier studies which suggest that fine-grained aggregates, with broad grain size distributions, perform better[17,31,43,30].

Interestingly, when aggregates are grouped by RHD levels like presented in Table 4, ϕm becomes significantly (and negatively) correlated with BPN, especially in harder aggregates, suggesting that fine-grained rocks indeed offer superior resistance to polishing. This conclusion is supported by SEM micrographs, presented at Figure 12, of two facies of Gra3, which have the same mineralogical composition but different mean grain size (ϕm): the fine-grained facies exhibit a more pronounced surface texture compared to the medium-grained one. Correlation coefficients for σ, GSI, and CV remains generally weak or insignificant for hard aggregates, but stronger and negative for soft aggregates. This suggests that, among soft aggregates, those with more uniform grain sizes show greater resistance to projection polishing.

Table 4. Pearson correlation coefficients (r) between BPNf / ΔBPN and grain size and distribution properties, for different group of aggregates.

	Type of aggregates	ϕm	σ	CV	GSI
BPNf	**Hard aggregates (Gwk, Gra, Gns)**	-0.627	-0.619	0.019	0.105
ΔBPN		-0.418	-0.463	-0.312	-0.194
BPNf	**Soft aggregates (Bas, Dol, Lim)**	-0.334	-0.453	-0.379	-0.470
ΔBPN		-0.330	-0.452	-0.222	-0.843

Figure 12 : Scanning Electron Microscope (SEM) micrographs of the surface of representative particles of the fine (A) and medium-grained facies of the granodiorite, after 35 cycles of polishing, highlighting the effect of grain size: the fine-grained facies is more finely textured than the medium-grained.

A (Fine-grained granodiorite – ϕ=535.5 µm, 75X)

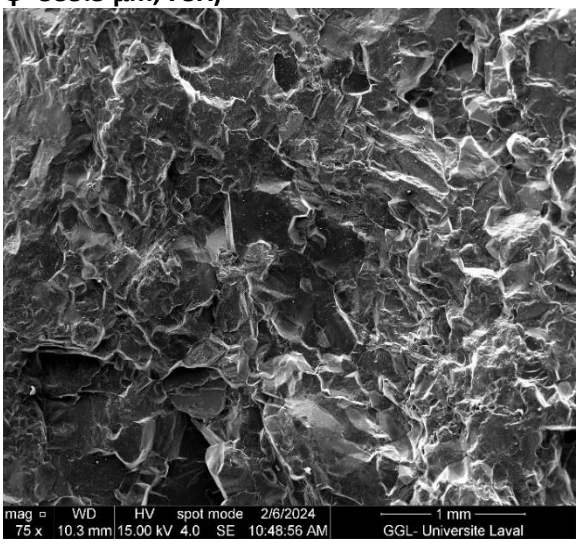

B (Medium-grained granodiorite - ϕ=1379.0µm, 75X)

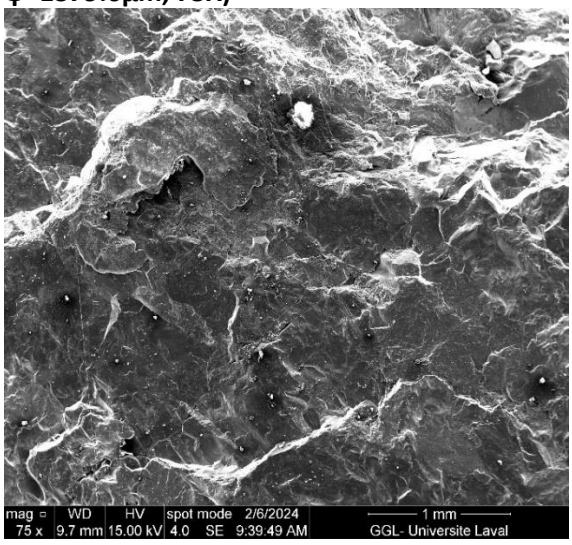

Table 5 presents the Pearson correlations between BPNf, ΔBPN and microtextural properties pre- (i) and post-polishing (f). Peak height H shows the strongest positive correlation, whereas peak density Np and shape α exhibit negative correlations. Notably, the final peak density (Npf) demonstrates the strongest correlation with BPNf. From that, it can be said that aggregates with numerous, tall and sharp peaks, exhibit a superior initial microtexture and retain that microtexture more effectively under polishing by projection.

Table 5 : Pearson correlation coefficients (r) between BPNf / ΔBPN and microtextural properties of the selected aggregates.

	Hi	**Hf**	**ΔH**	**αi**	**αf**	**Δα**	**Npi**	**Npf**	**ΔNp**
BPNf	0.751	0.745	0.429	-0.723	-0.714	-0.413	-0.710	-0.764	-0.405
ΔBPN	0.755	0.743	0.391	-0.731	-0.725	-0.430	-0.695	-0.718	-0.325

Prediction models

Table 6 presents the multiple linear regression models developed using the most influential aggregates properties identified earlier. R^2 represents the proportion of variability in BPNf explained by the models, while the adjusted R^2 ($R^2_{adj.}$) corrects this value by accounting for the number of explanatory variables included, providing a more robust measure of the models explanatory power. These models incorporate mineralogical, petrographic and microtextural properties to explain the evolution of polishing resistance. Model 1 includes only mineralogical and petrographic variables and achieves the highest coefficient of determination (R^2 = 0.94; $R^2_{adj.}$=0.92), confirming their predominant role. By integrating individual mineral contents, it operates at a finer level where each mineral contributes directly to polishing resistance. In contrast, Models 2 and 3 adopt a more aggregated approach by incorporating differential hardness (DH) and relative hardness (RHD), which synthesize the effects of several minerals and their Mohs hardness. These models also include microtextural parameters and explain 89% to 90% of the variability in polishing resistance ($R^2_{adj.}$ between 0.87 and 0.92), highlighting the added explanatory factor of microtextural variables. Also, all microtextural parameters used (in Models 2 and 3) are measured before polishing (i). Their association with mineralogical (RHD, DH) and petrographic properties (CV, ϕm) suggests that final polishing resistance is governed not only by the initial microtexture, but also by the intrinsic properties that control its evolution under polishing. All statistical validation procedures for the multiple linear regression models are detailed in a soon-to-be published article[44].

Table 6 : Proposed models.

N°	**Equations**	**R^2**	**$R^2_{adj.}$**
1	BPNf = 0.265***Qz** + 0.131***Pl** + 0.080***Dol** – 4.073 ***GSI**+ 43.587	0.94	0.92
2	BPNf = 1528.585***Hi** – 3.743***CV** – 0.007***ϕm** + 4.757***DH** + 36.730	0.90	0.87
3	BPNf = 2.906***RHD** + 3.668***DH** – 0.027***Npi** + 67.953	0.89	0.87

Notes: BPNf: British pendulum number after 35 cycles of polishing; Qz: quartz content; Pl: plagioclase content; Dol: dolomite content; GSI: Gini-style index; Hi: peak height before polishing; CV: coefficient of variation; ϕm: mean grain size; DH: differential hardness; RHD: relative hardness; Npi: peak density before polishing.

Conclusion

This study investigated the LC 21-102 standard test method, used in Quebec to assess the polishing resistance of aggregates. Specifically, it examined the effects of polishing by projection time, mechanisms and intrinsic aggregate properties on both polishing resistance and microtexture evolution across a range of natural aggregates. The findings reveal that:

- the conventional specimen-preparation procedure, which uses plaster as the first layer to fix the aggregate particles, leaves plaster residues embedded in the peaks forming the microtexture and thus could interferes with microprofilometer analyses. A new preparation procedure was therefore adopted: the first layer of plaster is replaced with a layer of clean, coarse sand that is too large to be inserted into the microtexture.
- polishing by projection operates through a distinct mechanism compared to conventional methods such as the pneumatic and (W/S) polishing. It acts by digging into the aggregate surface, whereas the other two methods mainly involve grinding or crushing.
- the maximum wear of most aggregates is reached after approximately 35 polishing cycles and not 20, suggesting a need to revise test parameters to better reflect actual wear.
- mineralogical and petrographic properties such as RHD, DH and ϕm significantly influence microtexture evolution under polishing.
- Multiple linear regression models, incorporating mineralogical, petrographic, and microtextural parameters, were successfully developed to predict polishing resistance. These models demonstrate the interconnected role of these factors in microtexture deterioration and could allow for polishing resistance to be estimated without conducting physical tests, saving considerable time.

These results contribute to a deeper understanding of the LC 21-102 test mechanisms and parameters. Future research should focus on validating these results through field performance studies. In particular, correlations between laboratory-measured polishing resistance (at both 20 and 35 cycles) and in-service pavement performance should be established. Such findings could support revisions to the LC 21-102 test method, such as increasing the recommended number of cycles to ensure that the test outcomes reflect real-world conditions more accurately.

References

[1]J. W. Hall, K.L. Smith, L. Titus-Glover, J.C. Wambold, T.J. Yager, Z. Rado, Guide for pavement friction, NCHRP - National Cooperative Highway Research Program, 2009.
[2]S. de l'assurance automobile du Québec. SAAQ, "Bilan routier 2022 – Faits saillants", Bibliothèque et Archives nationales du Québec, 2023.
[3]Données Québec, Rapports d'accident - Données Québec, donneequebec.ca (2024). https://www.donneesquebec.ca/recherche/dataset/rapports-d-accident. (accessed February 19, 2024).
[4]Austroads, "AUSTROADS TECHNICAL REPORT: Road Surface Characteristics and Crash Occurrence: A Literature Review", Austroads, Sydney, Australie, (2008).
[5]BNQ-Bureau de Normalisation du Québec, "BNQ 2560-114: Travaux de génie civil - granulats", 2014.
[6]LC - Laboratoire des Chaussées, "LC 21-102: Résistance au polissage des granulats: Méthode par projection", (2019).
[7]Direction du Laboratoire des Chaussées, "Adhérence des chaussées en béton de ciment", (2007).

[8]M. Boulet, J.-C. Deffieux, G. Delalande, M.-T. Do, M. Gothié, Y. Goyat, "Mesures de l'adhérence des chaussées routières et aéronautiques", (Paris, France), Lab. Cent. Des. Ponts Et. Chaussées (2006) (Paris, France).
[9]B. Guan, J. Wu, C. Xie, J. Fang, H. Zheng, H. Chen, Influence of macrotexture and microtexture on the skid resistance of aggregates, Adv. Mater. Sci. Eng. 2018 (2018) 1–9, https://doi.org/10.1155/2018/1437069.
[10]M.-T. Do, M. Kane, Z. Tang, F. de Larrard, Physical model for the prediction of pavement polishing, *Wear*, 267 (2009) 81–85, https://doi.org/10.1016/j. wear.2008.11.012.
[11]C. Tourenq, D. Fourmaintraux, "Propriétés des granulats et glissance routière", Bulletin De Liaison du Laboratoire Des Ponts Et Chaussées (1971).
[12]CEN - Comité Européen de Normalisation, "EN 1097-8: Tests for mechanical and physical properties of aggregates - Part 8: Determination of the polished stone value", (2020).
[13]Australian Standard, "AS 1141.40: Methods for sampling and testing aggregates Method 40: Polished aggregate friction value - Vertical road-wheel machine", (2017).
[14]M. Kane, I. Artamendi, T. Scarpas, Long-term skid resistance of asphalt surfacings: correlation between Wehner–Schulze friction values and the mineralogical composition of the aggregates, *Wear,* 303 (2013) 235–243, https://doi.org/ 10.1016/j.wear.2013.03.022.
[15]LC - Laboratoire des Chaussées, "LC 21-102: Résistance au polissage des granulats: Méthode par projection", (2019).
[16]G. Delalande, Résistance des granulats par polissage: méthode d'essai par projection, Laboratoire Régional des Ponts et Chaussées, Angers, (1992).
[17]S. Julien, G. Tremblay, M.-A. Bérubé, B. Auger, Relation entre la nature des granulats et la glissance des chaussées, in: 1994: pp. 114–133.
[18]A. Bédard, Influence réciproque de la macrotexture et de la microtexture sur l'adhérence des revêtements routiers, Université Laval, Québec, 1999.
[19]M.T. Do, P. Marsac, Assessment of the Polishing of the Aggregate Microtexture by Means of Geometric Parameters, in: TRB 81st Annual Meeting (Transportation Research Board), France, 2002: pp. 19p, schémas, graphiques, tabl.ill.bibliogr. https://hal.science/hal-00851293, (accessed March 13, 2024).
[20]S. Julien, G. Tremblay, M.-A. Bérubé, B. Auger, Évaluation de la résistance au polissage des granulats à l'aide d'essais de laboratoire, in: Québec, 1994: pp. 256–282.
[21]M. Perreault, G.L. Bourque, ´Évolution du transport routier au Québec; La crise d'un paradigme, Gouvernement du Québec, Institut de recherche en économie contemporaine, 2014.
[22]IGO2-Données Québec, (n.d.). https://geoegl.msp.gouv.qc.ca/igo2/apercu-qc/?context=mtq&visiblelayers=circulation_routier,bgr_mtq_annotation, (accessed February 16, 2025).
[23]R. et S. SOM, *Sondage Omnibus téléphonique sur l'utilisation des pneus d'hiver à crampons et la notoriété du service Québec 511*, 2014.
[24]J. Lambert, S. Lessard, Rapport du Vérificateur général du Québec à l'Assemblée nationale pour l'année 2021-2022, *Rapport de la commissaire au développement durable, Chapitre 4: Sels de voirie: optimiser leur usage pour en limiter les répercussions sur l'environnement*, Gouvernement du Québec, Québec, 2022.
[25]S. Shabani, M. Ahmadinejad, M. Ameri, Developing a model for estimation of polished stone value (PSV) of road surface aggregates based on petrographic parameters, *International Journal of Pavement Engineering,* 14 (2013) 242–255, https://doi.org/10.1080/ 10298436.2012.693179.
[26]M. Kane, V. Edmondson, Long-term skid resistance of asphalt surfacings and aggregates' mineralogical composition: Generalisation to pavements made of different aggregate types, *Wear,* 454–455 (2020) 203339, https://doi.org/10.1016/ j.wear.2020.203339.
[27]M.-T. Do, Z. Tang, M. Kane, F. de Larrard, Evolution of road-surface skid-resistance and texture due to polishing, *Wear*, 266 (2009) 574–577, https://doi.org/10.1016/ j.wear.2008.04.060.

[28]A.D. Nataadmadja, M.T. Do, D.J. Wilson, S.B. Costello, Quantifying aggregate microtexture with respect to wear—Case of New Zealand aggregates, Wear 332–333 (2015) 907–917, https://doi.org/10.1016/j.wear.2014.11.028.

[29]M.J. Perry, Role of aggregate petrography in micro-texture retention of greywacke surfacing aggregate, Road. Mater. Pavement Des. 15 (2014) 791–803, https://doi. org/10.1080/14680629.2014.923781.

[30]D. Wang, P. Liu, M. Oeser, H. Stanjek, and J. Kollmann, 2019. Multi-scale study of the polishing behaviour of quartz and feldspar on road surfacing aggregate. *International Journal of Pavement Engineering*, 20 (1), 79–88.

[31]N. Roy, K.K. Kuna, Influence of aggregate mineral grain size and size distribution on pavement surface microtexture deterioration, *Journal of Transportation Engineering*, *Part B: Pavements,* 150 (2024) 04024014, https://doi.org/10.1061/JPEODX.PVENG-1422.

[32]LC - Laboratoire des Chaussées, LC 21-070: Détermination du pourcentage d'usure par attrition du gros granulat au moyen de l'appareil Micro-Deval, (2021).

[33]LC - Laboratoire des Chaussées, LC 21-400: Détermination de la résistance à l'abrasion au moyen de l'appareil Los Angeles, (2021).

[34]C. Klein, B. Dutrow, and J. Dwight, 2008. The 23rd edition of the manual of mineral science (after James D. Dana). 23rd ed. New York : J. Wiley & Sons, cop. 2008.

[35]M.C. Brown, 1994. Using gini-style indices to evaluate the spatial patterns of health practitioners: Theoretical considerations and an application based on Alberta data. *Social Science & Medicine*, 38 (9), 1243–1256.

[36]CEN - Comité Européen de Normalisation, 2011. EN 13036-4: Road and airfield surface characteristics. Test methods - Method for measurement of slip/skid resistance of a surface: The pendulum test.

[37]M. Kandji, B. Fournier, J. Duchesne, and F. Doucet, 2025. Effect of polishing time, mechanisms and mineralogy on the microtexture evolution and polishing resistance of pavement surface aggregates. *Construction and Building Materials*, 476, 141105.

[38]N. Roy, S. Sarkar, K.K. Kuna, S.K. Ghosh, Effect of coarse aggregate mineralogy on micro-texture deterioration and polished stone value, *Construction and Building Materials,* 296 (2021) 123716, https://doi.org/10.1016/j.conbuildmat.2021.123716.

[39]A.M. Dunford, A.R. Parry, P.H. Shipway, H.E. Viner, Three-dimensional characterisation of surface texture for road stones undergoing simulated traffic wear, *Wear,* 292–293 (2012) 188–196, https://doi.org/10.1016/j. wear.2012.05.010.

[40]R. Vaiana, F. Balzano, T. Iuele, V. Gallelli, Microtexture performance of EAF slags used as aggregate in asphalt mixes: a comparative study with surface properties of natural stones, *Applied Sciences,* 9 (2019) 3197, https://doi.org/10.3390/app9153197.

[41]J. Lei, N. Zheng, X. Chen, J. Bi, X. Wu, Research on the relationship between anti- skid performance and various aggregate micro texture based on laser scanning confocal microscope, *Construction and Building Materials,* 316 (2022) 125984, https://doi.org/ 10.1016/j.conbuildmat.2021.125984.

[42]Y. Zong, R. Xiong, Z. Wang, B. Zhang, Y. Tian, Y. Sheng, C. Xie, H. Wang, X. Yan, Effect of morphology characteristics on the polishing resistance of coarse aggregates on asphalt pavement, *Construction and Building Materials,* 341 (2022) 127755, https:// doi.org/10.1016/j.conbuildmat.2022.127755.

[43]D. Wang, X. Chen, Xie, X., Stanjek, H., Oeser, M., and Steinauer, B., 2015. A study of the laboratory polishing behavior of granite as road surfacing aggregate. *Construction and Building Materials*, 89, 25–35.

[44]M. Kandji, B. Fournier, J. Duchesne, and F. Doucet, 2025. Influence of the intrinsic properties of pavement surface aggregates on skid resistance: development of a predictive model.